Iranian Journal of Oil & Gas Science and Technology, Vol. 9 (2020), No. 3, pp. 102–115
http://ijogst.put.ac.ir

Identifying Gas-bearing Carbonate Reservoir Using Extended Elastic Impedance

Hessam Mansouri Siahgoli[1], Mohammad Ali Riahi[2*], Bahare Heidari[3], and Reza Mohebian[4]

[1]Ph.D. Candidate, Institute of Geophysics, University of Tehran, Tehran, Iran
[2]Professor, Institute of Geophysics, University of Tehran, Tehran, Iran
[3]M.S. Student, Institute of Geophysics, University of Tehran, Tehran, Iran
[4]Geophysics Expert, KPE Co., Tehran, Iran

Highlights

- Extended elastic impedance (EEI) can be used as a seismic reconnaissance attribute with the ability to predict reservoir fluids and lithology.
- EEI allows for a better distinction between seismic anomaly caused by lithology and the one caused by the fluid content.
- Recognizing gas-bearing intervals by applying the EEI will ultimately reduce the drilling risk and cost in areas with carbonate reservoirs.
- Application of EEI leads to the more reliable estimation of porosity and fluid saturation in carbonate reservoirs.
- The proposed methodology illustrates the advantage of using $\lambda\rho$ and $\mu\rho$ for discriminating the reservoir rock properties, as compared to the conventional *Vp* and *Vs* analysis.

Received: February 06, 2020; *revised*: April 16, 2020; *accepted*: April 28, 2020

Abstract

It is difficult to identify the carbonate reservoirs by using conventional seismic reflection data, especially in cases where the reflection coefficient of the gas-bearing zone is close to that of the carbonate background. In such cases, the extended elastic impedance (EEI) as a seismic reconnaissance attribute with the ability to predict fluids and lithology can be used. It allows for a better distinction between seismic anomaly caused by lithology and the one caused by the fluid content. The EEI attribute extends the available reflection angles and applies different weights to the intercept and gradient values so as to extract the petrophysical properties of the rock at a specific incident angle. Using the EEI attribute, we can estimate the elastic parameters such as shear impedance; the ratio of the compressional velocity to shear velocity; Poisson's ratio; and bulk, Lame, and shear moduli, and petrophysical properties, including porosity, clay content, and water saturation. The known reservoirs in the study area are three oil-bearing formations namely, Surmeh (Arab), Gadvan (Buwaib), and Dariyan (Shuaiba), and three gas-bearing formations, including Kangan, Dalan, and Faraghan. The Dehram group is composed of Kangan (Triassic), Dalan, and Faraghan (Permian) formations. Permian carbonates of Kangan–Dalan and its equivalent Khuff have regionally been developed as a thick carbonate sequence in the southern Persian Gulf region. In this paper, parameters λp and $\mu\rho$ extracted from the EEI method are used to characterize a carbonate reservoir. Our results show that the EEI can highlight the difference between the reservoir and non-reservoir formation to identify the gas-bearing areas.

Keywords: Extended Elastic Impedance, Inversion, Carbonate Reservoirs, Gas-bearing

* Corresponding author:
Email: mariahi@ut.ac.ir

How to cite this article
Mansouri Siahgoli H, Riahi M A, Heidari B, Mohebian R, Identifying Gas-bearing Carbonate Reservoir Using Extended Elastic Impedance. Iran J. Oil Gas Sci. Technol., Vol. 9, No. 3, p. 102–115, 2020.
DOI: 10.22050/ijogst.2020.218837.1535

1. Introduction

Due to the lower susceptibility of the S-wave to the presence of gas, the S-wave reflection data could be considered as significant tools for detecting gas bearing intervals in carbonate reservoirs (Ensley, 1984). Based on this concept, recording S-wave data along with the P-wave data is a necessity. However, the high cost of S-wave acquisition and processing pushes many geophysicists to continue using standard methods such as the amplitude versus offset (AVO), the application of which is expected to compensate for the absence of the S-wave data. In a general sense, the AVO method is categorized into two different scopes: the seismic reflectivity and the impedance methods (Figure 1).

Whitecombe et al. 2002 have applied the EEI approach based on Connolly's (1999) method of the elastic impedance (EI). They expanded the conventional EI for all the values of $\sin^2\theta$ between negative and positive infinity using equation $\sin^2\theta = \tan\chi$, where the term $\sin^2\theta$ was replaced by the term $\tan\chi$. Their research shows that the logs extracted from the EEI at specific angles are related to shear, bulk, and Lame moduli. In another work, Neves et al. (2004) expressed how the EEI approach could be employed to estimate petrophysical logs. Their study was performed on a gas reservoir in central Saudi Arabia. Also, Hyeonju et al. (2015) performed the EEI inversion method to predict density, porosity, and gamma-ray values of the Second Wall Creek Sand, the Teapot Dome field, Wyoming, the USA. In (2017) Samba et al. investigated the prediction of reservoir properties using extended elastic impedance for the case of Nianga field of West African Congo basin. Chehrazi and Albouyeh (2018) applied EEI Inversion to reservoir from non-reservoir discrimination of Ghar reservoir in one Iranian oil field within Persian Gulf.

The current work aims to use the rock physics analysis of well log data and the λ-μ-ρ attributes from the AVO inversion of 3D seismic data to discriminate the lithology from fluid properties. We test this method for the characterization of a gas interval in an Iranian carbonate reservoir. The field of study is one of the Iranian oil fields, located in the southwest of Iran, and the target layer is Kangan formation. The quality of data is good, and the accuracy of well ties is about 82%.

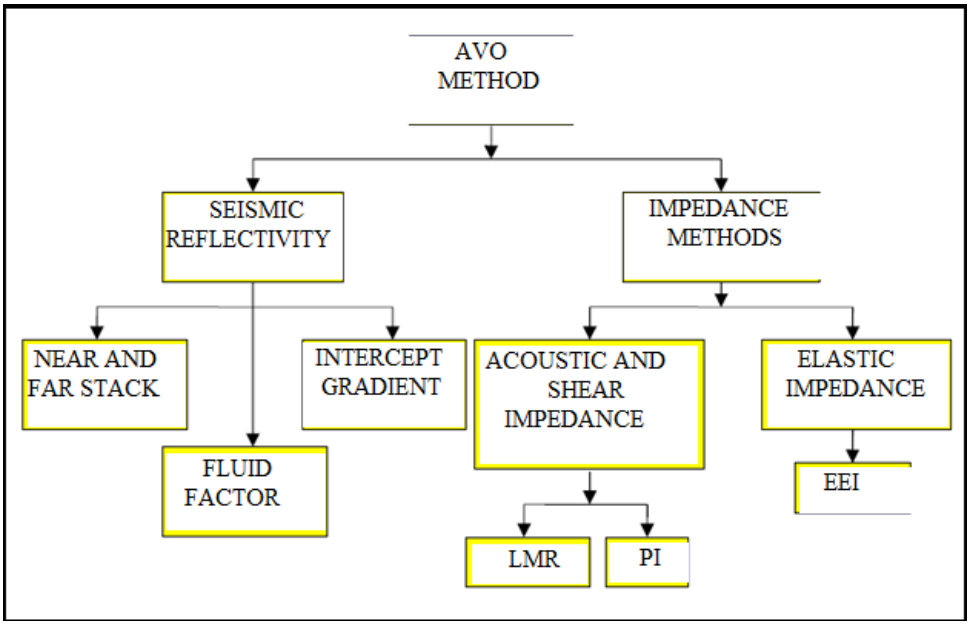

Figure 1

A schematic categorization of the AVO methods and the pre-stack seismic inversion (Russell and Russell, 2012).

2. Definition

Theoretically, the intercept and gradient values in the linearized Zoeppritz equation (Equation (1)) can be combined with any desired weight (Aki and Richards, 1980).

$$(\theta) \approx A + Bsin^2\theta$$
$$A = \frac{1}{2}\left[\frac{\Delta Vp}{Vp} + \frac{\Delta \rho}{\rho}\right] \quad (1)$$
$$B = \frac{1}{2}\frac{\Delta Vp}{Vp} - 2\left(\frac{Vs}{Vp}\right)^2 \left(2\frac{\Delta Vs}{Vs} + \frac{\Delta \rho}{\rho}\right)$$

For nonphysical values of θ, i.e. $\sin^2\theta < 0$ or $\sin^2\theta > 1$, the linear approximation of $R(\theta)$ versus $\sin^2\theta$ over the range of linear observations is extended to reconstruct reflections for all the values of $\sin^2\theta$ (Figures 2 and 3).

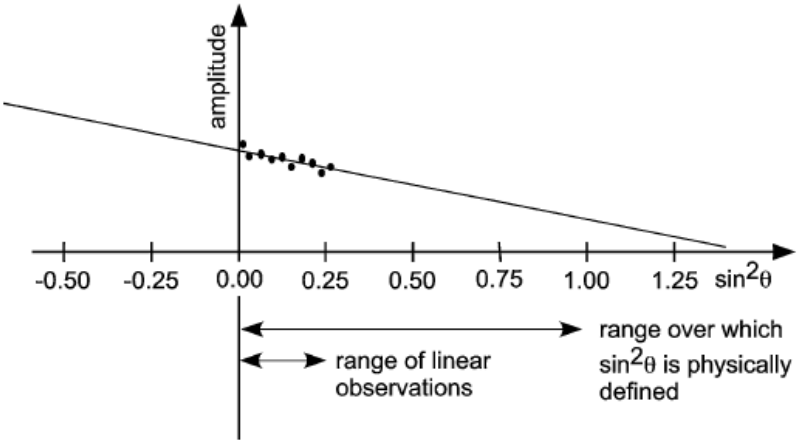

Figure 2

Widening the range of angles for the EEI method; the linear model can be extrapolated beyond the range of the measured data and beyond the range over which $\sin^2\theta$ is physically definable (Whitecombe et al., 2002).

Based on the above conception Whitecombe et al. (2002) have suggested the proper shear wave reflection equation and the EEI relation as given below:

$$Rs = Acos\chi + Bsin\chi \quad (2)$$

where *A* and *B* are the intercept and gradient of the AVO respectively.

$$EEI\ (\chi) = \alpha 0\ \rho 0\ \left[\left(\frac{\alpha}{\alpha 0}\right)^P \left(\frac{\beta}{\beta 0}\right)^q \left(\frac{\rho}{\rho 0}\right)^r\right]$$
$$p = (cos\chi + sin\chi)$$
$$q = -8ksin\chi \quad (3)$$
$$r = (cos\chi - 4)$$

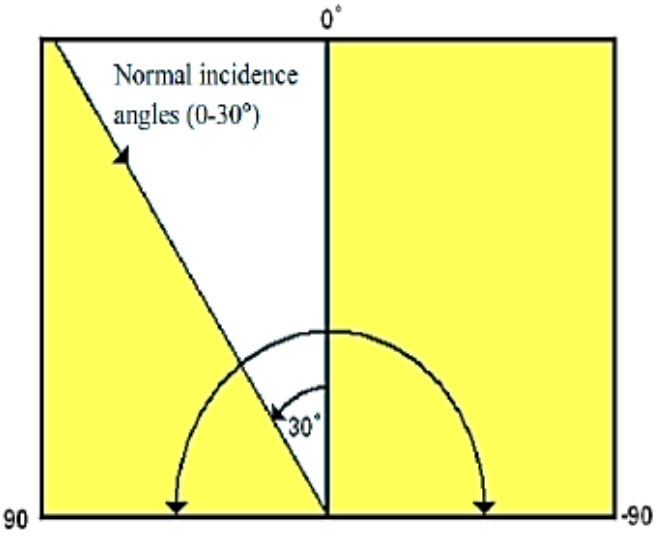

Figure 3

Angle χ is the extension of the reflectivity angle to a range of –90° to +90°; the values of $sin^2\,\theta$ are physically realizable in the range of 0–30° (Hampson and Russell, 2007).

Three other useful attributes that can be extracted from the results of pre-stack inversion are Lambda-Rho ($\lambda\rho$), Mu-Rho ($\mu\rho$), and Lambda–Mu ratios (LMR). The Lambda-Rho, referred to as the "LR" attribute, and Mu-Rho, known as "MR" attribute, are extracted from the P-impedance (Z_p) and the S-impedance (Z_s) cubes or well data using the following equations:

$$\text{Lambda-Rho: } \lambda\rho = Z^2_P - 2Z^2_S \tag{4}$$

$$\text{Mu-Rho: } \mu\rho = Z^2_S \tag{5}$$

2.1. Methodology

Goodway et al. (1997) and Li and Downton (2000) used the LMR method to estimate porosity and detect gas in a reservoir. Li and Downton (2000) showed that the presence of gas changed the elastic properties of carbonates, and the seismic amplitude increases in the presence of gas. Li et al. (2003) revealed advanced applications of the AVO method in carbonate rocks.

By inserting the values of the P-wave and S-wave and raising the density-corrected logs in Equation (3) in an angle range of −90 to +90°, a section of the EEI spectrum is computed. This can be performed either in MATLAB or using commercial software.

To find the optimum angle of χ, the log of a desired well is cross-correlated with the EEI spectrum section to find the specific χ at which the correlation is maximum. This procedure is repeated for all the logs.

The conventional angle gathers are first generated for the intercepts and gradients using industrial software. Then, by replacing the value of the optimum angle (χ) for each parameter in Equation (2), the reflectivity coefficient section is calculated for each desired parameter. The EEI attribute is also determined for the optimum angle. The same procedure is performed for angles corresponding to the desired parameters.

The 3D seismic data have good quality all over the study area. However, it should be mentioned that even after reprocessing, data quality does not improve below Kangan formation due to the acquisition

parameters. The seismic data are close to the minimum phase in the reservoir interval, and a pick in the seismic section for this interval corresponds to an increase in the acoustic impedance.

Figure 4 illustrates the quality and continuity of the seismic data at a time slice of 1150 ms. In this figure, the Gadvan (Lower-Buwaib) horizon is shown in green. The studied wells are displayed in the middle of the figure. Also, the quality of the seismic data is acceptable for the inversion (EEI) methodology.

After the low-frequency model is created, the inversion parameters are applied to the seismic section. These parameters are obtained based on the initial model and the extracted wavelet. This procedure is applied to all the sections related to other optimum angles.

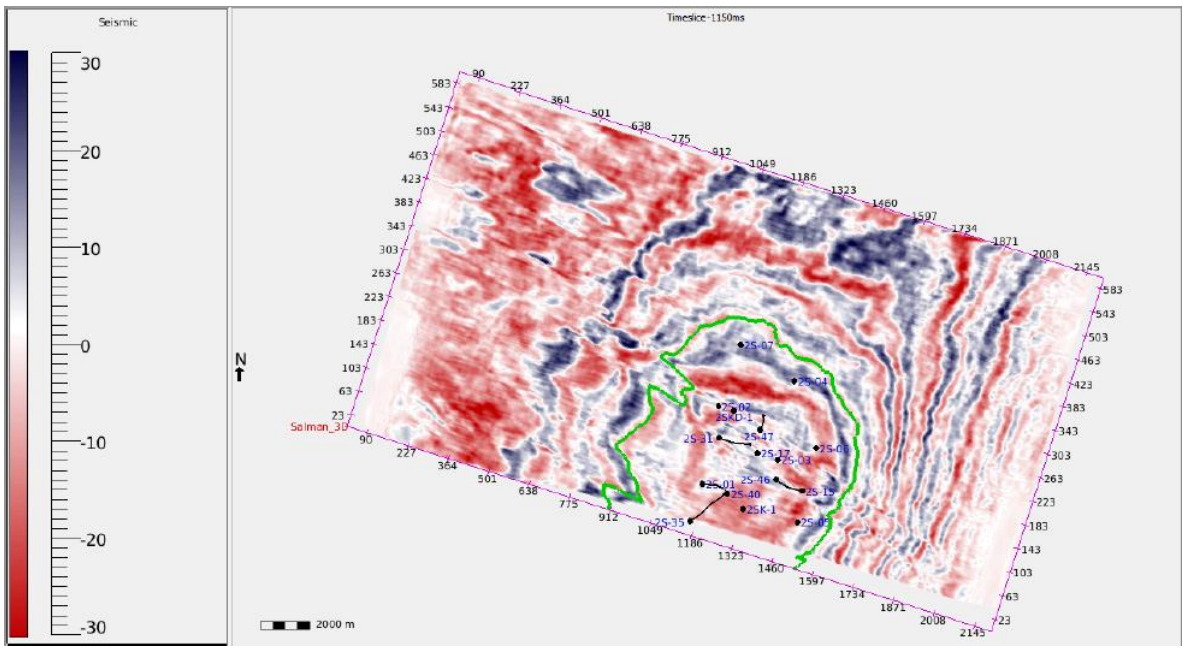

Figure 4

Seismic data at a time slice of 1150 ms; Gadvan (Lower-Buwaib) horizon is shown in green.

a. Geological setting

The oil field under study is located in the southwest of the Persian Gulf. The oil-bearing formations in the oil field include Surmeh (U.A.E.; Arab), Gadvan (U.A.E.: Buwaib), and Dariyan (U.A.E.: Shuaiba), and the gas-bearing horizons consist of Faraghan, Kangan, and Dalan formations (Dehram Group). The Dalan–Kangan Permo-Triassic age formations were deposited in a shallow-water carbonate ramp (Husseini, 1992; Al- husseini, 2000; Ghazban, 2007). The Dalan–Kangan formation plays a vital role in the Persian Gulf and is one of the world's most significant gas reservoirs. The type section of this formation has been reported from the subsurface information of southern Iran. Lithological changes of Kangan–Dalan formation are similar throughout the Persian Gulf; it includes limestone, dolomite, anhydrite, and shale. The upper part of Kangan formation consists of a sequence of inter-bedded red-to-green shales with cream-to-light-gray, sucrosic, anhydritic dolomites. The middle and the lower parts are composed of a series of dolomite and limestone. Dalan formation is a carbonate deposition of late Permian age. Lithologically, the formation could be divided into three sections, namely upper-carbonates, middle-carbonates, and lower-carbonates. The upper-carbonates consist of a cyclic sequence of limestone and dolomite. Some anhydritic layers are recognized in the middle part of the upper-carbonates, below which the limestone dolomite cycle is repeated. The middle anhydrates are a

mixture of anhydrates, dolomites, and oolitic dolomites, which act as a cap rock for the lower-carbonates. The lower-carbonates are shaly limestones at the top and dolomite and shaly pyrite in the middles. At the bottom of the lower-carbonates, the rock is similar to the shale texture of the middle anhydrate (Nairn and Alsharhan, 1997; Ghazban, 2007).

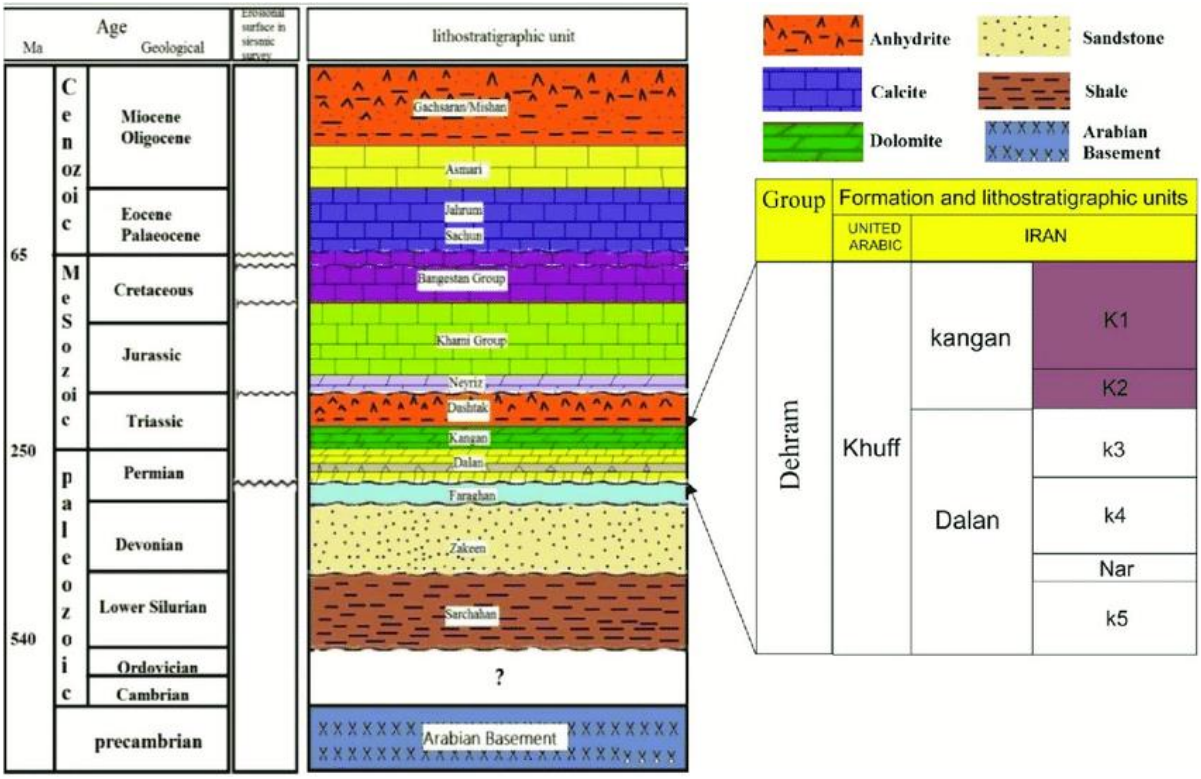

Figure 5

A generalized stratigraphic column of the study area; the gas production interval contains the upper Dalan and Kangan carbonates (Khuff equivalents) (Kadkhodaie et al., 2019).

b. Case study

The seismic data used in this study belong to a carbonate reservoir, and one of the seismic inline is shown in Figure 6. The reservoir formation is described as a quite thick-bedded limestone interval with few dolomitic beds between 1720 and 1800 ms (see Figure 7). Referring to this figure, the variation in the *Vp* and *Vs* logs and the decrease in the ratio of *Vp* to *Vs* in the specified interval will help us to detect the fluid presence.

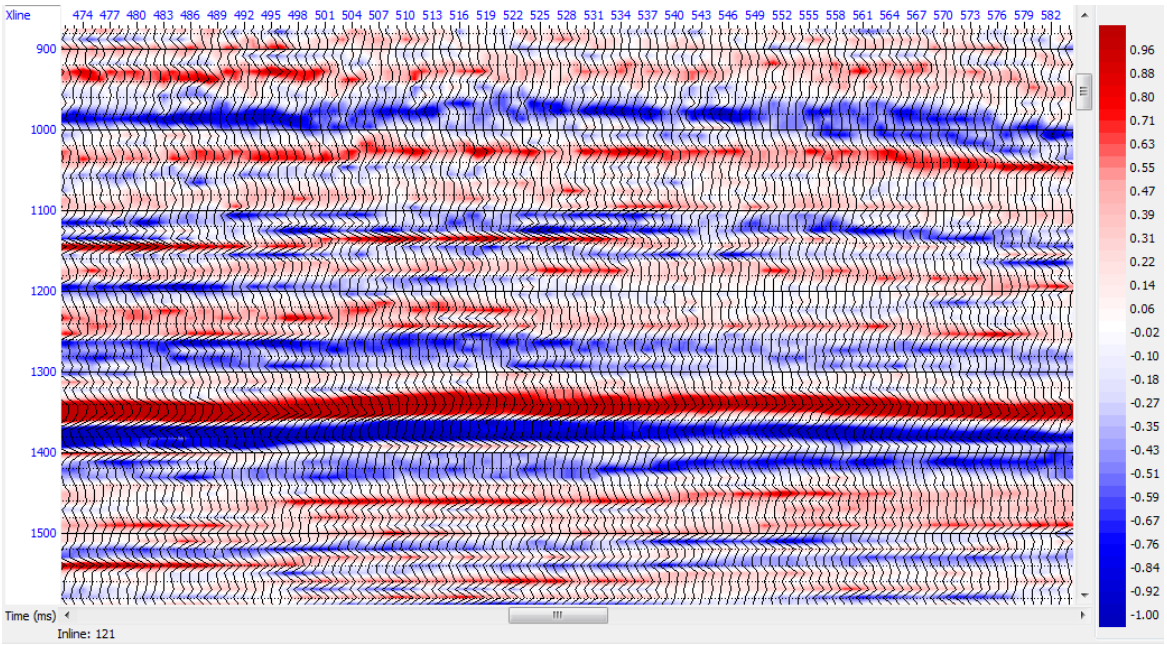

Figure 6

Post-stack section of seismic data.

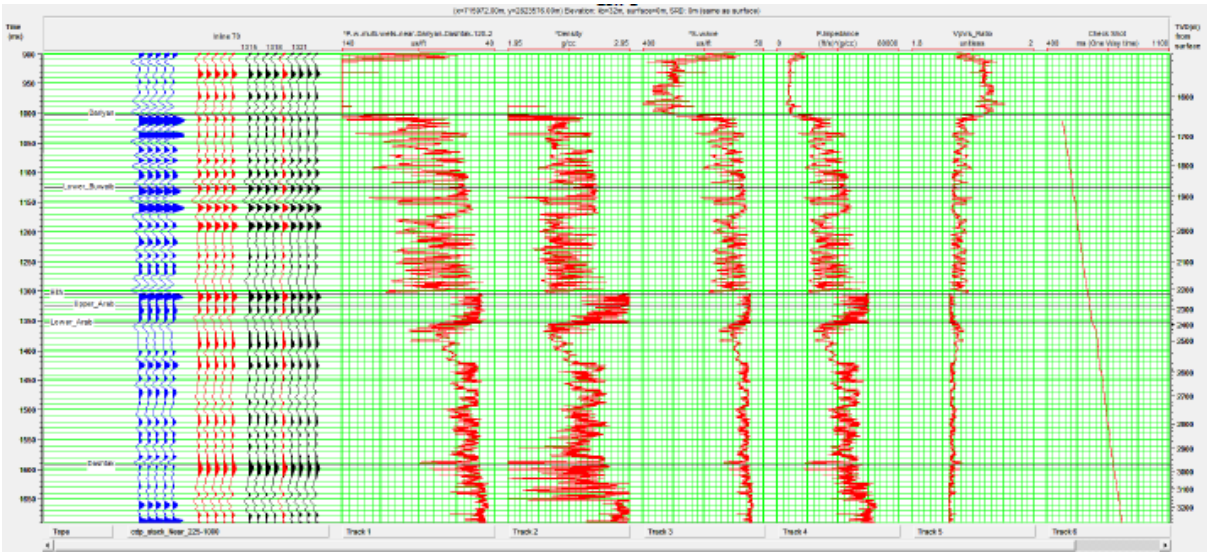

Figure 7

Synthetic seismogram, P-wave, S-wave, and Vp/Vs in the reservoir interval are extracted from a well and the seismic data at the well location.

For parameters like vp/vs, $\lambda\rho$, and $\mu\rho$, which are suitable fluid indicators, the optimum angle is obtained as illustrated in Figure 8. The related EEI logs are then calculated and shown in Figure 9; as the final step, by having an initial model and applying the inversion method, two sections for $\lambda\rho$ and $\mu\rho$ are obtained. The resulted sections show a proper correlation with their original logs, as depicted in Figures 10 and 11.

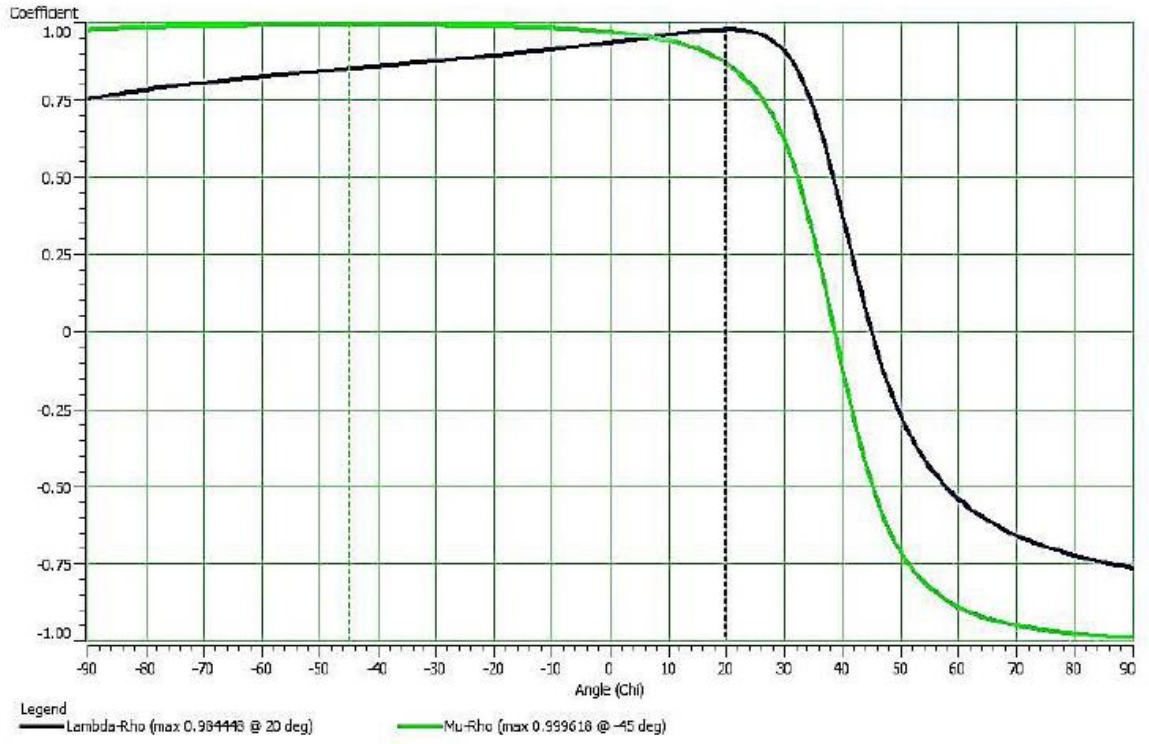

Figure 8

The correlation coefficient for the λp and $\mu\rho$ logs correlated with the EEI spectrum section; for these data, the maximum correlation is obtained at 20 and –45°.

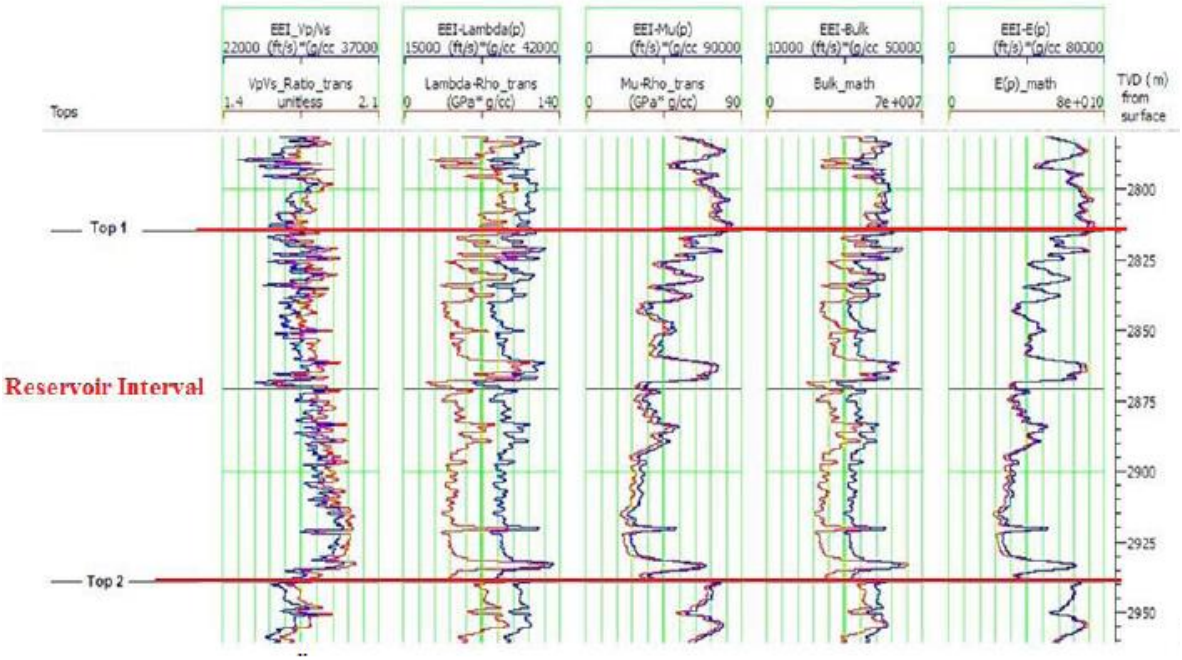

Figure 9

The well logs of vp/vs, λp, $\mu\rho$, K, and $E\rho$ along with their calculated EEI log at their specific optimum angle.

As mentioned above, λp is one of the best fluid indicators. It decreases sharply in the presence of fluids, especially in gas-bearing zones. Therefore, by plotting its impedance sections, we could discriminate

against the possible location of hydrocarbon occurrence (Figure 10).

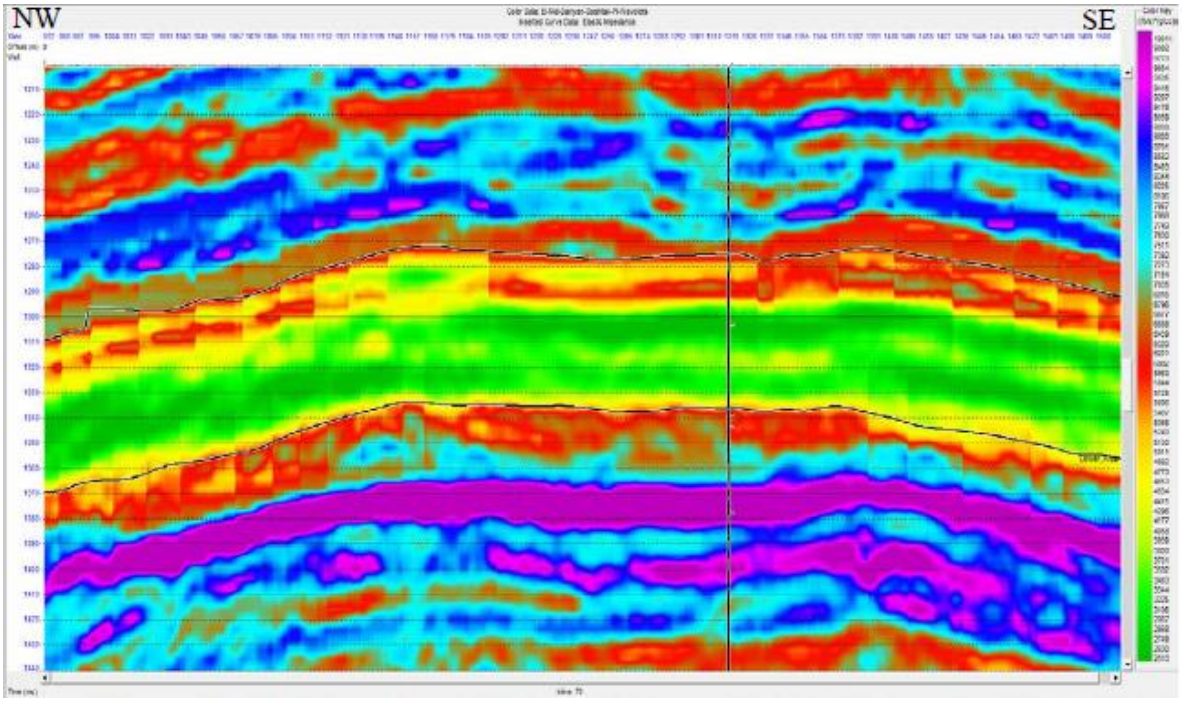

Figure 10

$\lambda\rho$ attribute at a χ of 20°; a lower value of this attribute in the target interval indicates the presence of gas.

Subsequently, $\mu\rho$ as another indicator that can be used to detect a gas reservoir is shown in Figure 11; this indicator, which is sensitive to lithology, starts to increase in the hydrocarbon area, especially in the presence of gas; this issue is displayed in Figure 11.

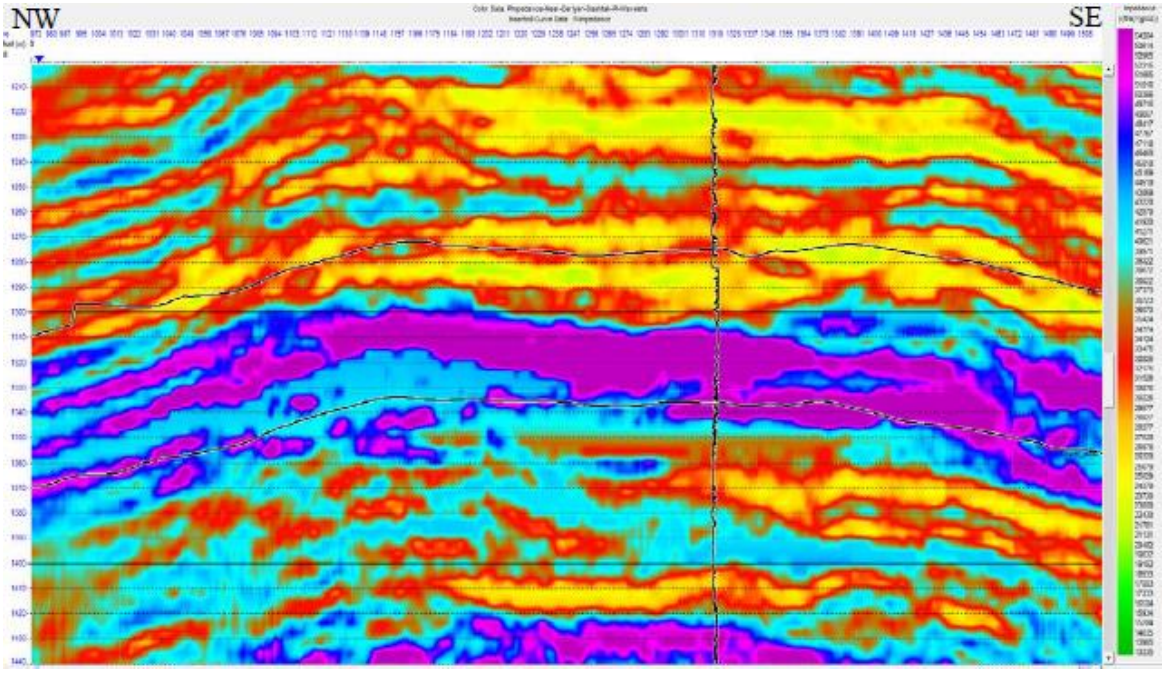

Figure 11

$\mu\rho$ attribute at a χ of –45°; this attribute increases in the presence of gas.

Lame parameters (Lambda-Rho and Mu-Rho) are the two most important parameters for the identification of the fluids and reservoir rocks. Lambda-Rho is sensitive to the fluid content of the rock fabric, while Mu-Rho is only sensitive to the rock matrix. The combination of these attributes allows a more accurate separation of the effects of the rock and the fluid in the reservoir. In the pre-stack seismic inversion, after the generation of the final P-impedance, S-impedance, *Vp*, *Vs*, *Vp*/*Vs*, and density cubes, the Lambda-Rho, Mu-Rho, and Lambda–Mu ratios are determined for two inversion time gates. The results of final pre-stack inversion for two inversion time gates are rendered in the following subsections (Figure 12):

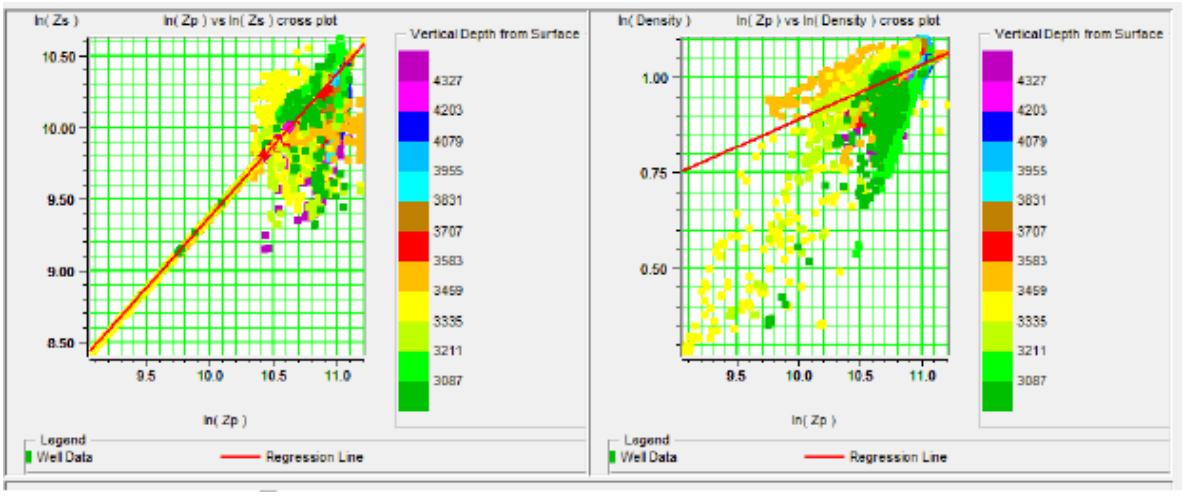

Figure 12

Cross-plots of ln(Z_s) versus ln(Z_p) (on the right) and ln(density) versus ln(Z_p) (on the left), showing the two relations obtained from the used wells for the upper inversion time gate.

Furthermore, it is confirmed that, contrary to sandstone reservoirs, the indicated reservoir interval cannot be easily detected by the cross-plot method. The reason for this is that in the case of sandstone reservoirs, the clusters follow a specific, predictable trend, while in carbonate reservoirs, drawing a separating line to recognize the hydrocarbon-bearing zones from the water-bearing zones is almost impossible in most cases. Therefore, such defects can illustrate the advantages of the EEI method.

3. Results

From Figures 7–11, the following can be inferred. In the gas-bearing interval, specifically where gas is present, a sudden reduction in the vp/vs ratio is evident. Hence, a reasonable correlation can exist between the lower values of the vp/vs ratio and the presence of gas in the reservoir. Moreover, in the presence of gas, $\lambda\rho$ declines, while $\mu\rho$ increases due to an increase in the fluid content and thus the porosity (see Figures 10 and 11).

The results of the elastic impedance are more reliable in Dariyan to Dashtak formations as compared to the deeper formations. This is because the seismic quality diminishes at deeper targets, which is intrinsic to wave propagation. A remedy to this will be to optimize the seismic acquisition parameters and increase the seismic resolution by sampling more frequently, that is, sampling every 2 ms instead of every 4 ms, which consequently leads to the better quality of the seismic data.

3.1. Discussion

According to the concepts of incompressibility and rigidity, as expressed by $\lambda\rho$ and $\mu\rho$ respectively, different types of lithologies tend to separate along orthogonal boundaries in a cross-plot of $\mu\rho$ versus $\lambda\rho$. As a result, these two parameters may be considered independent and can be interpreted separately. In combination, they provide additional information on the nature and content of the rocks and fluids from which they arise. This is a significant improvement over previous techniques for identifying gas accumulations, including the cross-plot of S-wave velocity versus P-wave velocity or the cross-plot of Poisson's ratio versus P-wave velocity, where both parameters must be interpreted at the same time. In particular, rock property sections of Lambda-Rho and Mu-Rho are interpreted by identifying zones of interest using one of them, and then the other is used to choose the original interpretation. For example, zones of low incompressibility ($\lambda\rho$) suggest the presence of gas or coal. Thus, by using the additional information available from the rigidity ($\mu\rho$), gas sands can be more clearly distinguished from coals because sand has high rigidity, and coal has low rigidity (Gray and Andersen, 2001).

Deeper seismic targets need long-offset acquisition settings to be properly imaged. Since the layers of the gas-bearing reservoirs in this field are deep, the offset of the seismic data is not long enough to suitably image these layers. The quality of the results of the elastic inversion is better in Dariyan to Dashtak inversion time gate than in Dashtak to Faraghan inversion time gate. This is chiefly due to the loss of the frequency content of the seismic data, the necessity of setting optimum acquisition parameters for deep reservoirs, and the lower quality of well-log data on the deeper layers of the reservoirs.

3.2. Validation of results

The results of this study are compared with other data such as drill stem test (DST), and their accuracy is validated by these results. The purpose of this paper is to find gaseous hydrocarbons in the carbonate reservoirs using the extended elastic impedance method, which is confirmed by the DST in areas where the results of the EEI indicate the presence of gas.

a. DST results

DST#1 is performed in the interval of 3561.5–3850 m in Kangan and upper Dalan formations. During the flowing period, the gas reaches the surface after 5 minutes. Then, the tool closes, and a closed-in tubing pressure of 4400 psig is recorded. The rates of gas are measured up to 32 mmscf/d with a condensate gas ratio (CGR) of 20 bbl/mmscf which is near the CGR of the representative pressure volume temperature (PVT) sample of this formation.

In DST#8, the testing interval is located in upper Dalan formation and contains a perforation interval, which is 12812 to 12910 ft. The test is conducted in tubing with a diameter of 3 1/2". In several stages of production and build, the bottom hole pressure is recorded at different choke sizes.

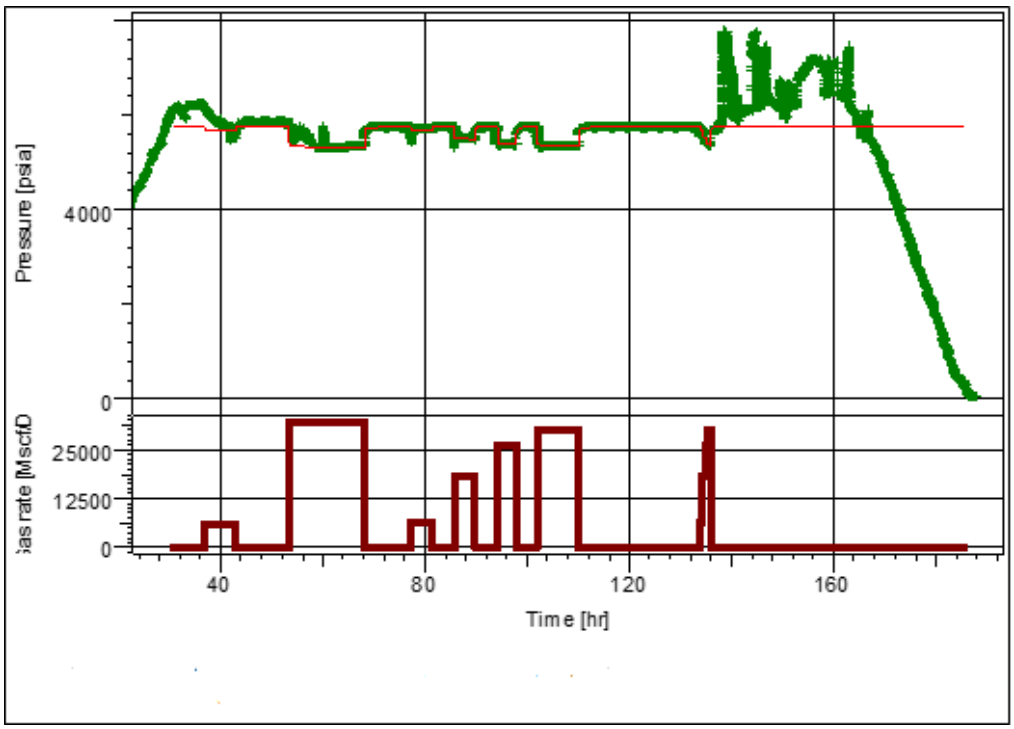

Figure 13

DST#1 history plot: pressure (psia), gas rate (mscf/D) versus time (h).

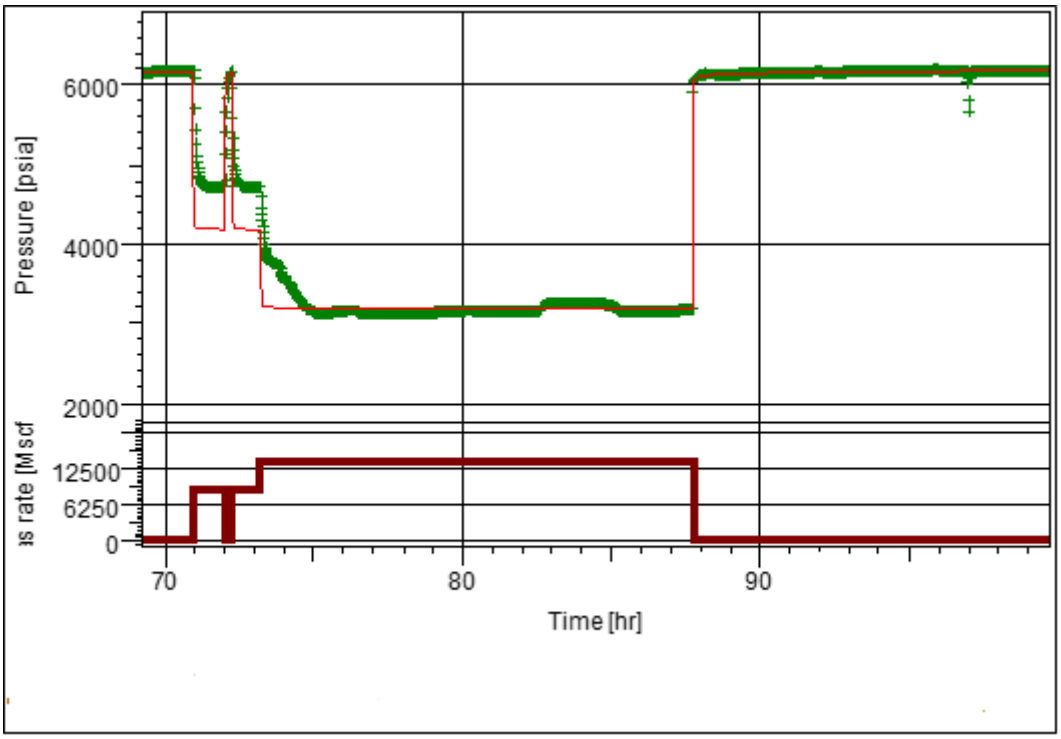

Figure 14

DST#8 history plot: pressure (psia), gas rate (mscf/D) versus time (h).

4. Conclusions

Recognizing gas-bearing intervals by applying the EEI method will ultimately reduce the drilling risk and cost in areas with carbonate reservoirs. This study illustrates the advantage of using $\lambda\rho$ and $\mu\rho$ for discriminating the reservoir rock properties, as compared to the conventional *Vp* and *Vs* analysis. The correlation between $\lambda\rho$ and $\mu\rho$ extracted from the inversion results with calculated logs at the well locations validates the superiority of our procedure for areas away from the well locations. Furthermore, this methodology leads to the more reliable estimation of porosity and fluid saturation in carbonate reservoirs. The results of this study indicate the suitable performance of the EEI method in detecting gas-bearing intervals in carbonate reservoirs.

The results of this study show that a reasonable correlation can exist between the lower values of the vp/vs and the presence of gas in the reservoir. $\lambda\rho$ values decrease while $\mu\rho$ values increase; the vp/vs decreases in the presence of gas, which is due to the increase of the fluid content.

Acknowledgements

The second author would like to appreciate the Research Council of the University of Tehran. This research did not receive any specific grant from funding agencies in the public, commercial, or not-for-profit sectors.

Nomenclature

EEI	Extended elastic impedance
E_d	Dynamic Young's modulus
K_d	Dynamic bulk modulus
μ	Shear modulus
ρ	Density
σ	Poisson's ratio
λ	Longitudinal modulus

References

Alhusseini, M.I., Origin of the Arabian Plate Structures: Amar Collision and Najd Rift, Geo Arabia, Vol. 5, No. 4, p. 527–542, 2000.

Aki, K. and Richards, P. G., Quantitative Seismology: Theory and Methods: W. H. Freeman and Co., 1980.

Russell B., and Russell H., CGG Veritas Company, an Overview of AVO and Inversion, 9th Biennial International Conference & Exposition, Petroleum Geophysics, 2012.

Chehrazi A., and Albouyeh M., Application of Extended Elastic Impedance (EEI) Inversion to Reservoir from Non-reservoir Discrimination of Ghar Reservoir in One Iranian Oil Field Within Persian Gulf, Journal of Geophysics and Engineering, Vol. 15, No. 4, p. 1204–1213, 2018.

Connolly, P., Elastic Impedance, The Leading Edge, Vol. 18, No.4, p. 438–452, 1999.

Ghazban F., Petroleum Geology of the Persian Gulf, Tehran University and National Iranian Oil Company, 2007.

Goodway, W., Chen, T., and Downton, J., Improved AVO Fluid Detection and Lithology Discrimination Using Lamé Petrophysical Parameter, CSEG RECORDER, Vol. 22, No. 7, p. 3–5, 1997.

Gray, D., and Andersen, E., The Application of AVO and Inversion to The Estimation of Rock Properties: Recorder, Vol. 26, No. 5, p. 36–40, 2001.

Ensley, R. A., Comparison of P- and S-Wave Seismic Data: A New Method for Detecting Gas Reservoirs: Geophysics, Vol. 49, No. 4, p. 1420–1431, 1984.

Hampson-Russell, Guide to Emerge: PDF in The Hampson-Russell Software Package, 2007.

Husseini, M.I., Upper Paleozoic Tectono-sedimentary Evolution of The Arabian and Adjoining Plates. Journal of The Geological Society of London, Vol. 149, No. 3, p. 419–429, 1992.

Hyeonju K., Gwang H. L., and Seonghoon M., Prediction of Reservoir Properties Using Extended Elastic Impedance Inversion, Economic and Environmental Geology, Vol. 48, No. 2, p. 115–130, 2015.

Kadkhodaie A, Nosrati A, Amini A, Chehrazi A, Mehdipour V, and Moslemnezhad T, Reservoir Properties Distribution in The Framework of Sequence Stratigraphic Units: A Case Study from The Kangan Formation, Iranian Offshore Gas Field, The Persian Gulf Basin, Journal of Natural Gas Science and Engineering, Vol. 65, p. 1–15, 2019.

Li, Y. Y., and Downton, J., Application of Amplitude Versus Offset in Carbonate Reservoirs: Reexamining the Potential, SEG Expanded Abstracts, p. 166–169, doi.org/10.1190/1.1815738, 2000.

Li, Y., Downton, J., and Goodway, B., Recent Applications of AVO to Carbonate Reservoirs in the Western Canadian Sedimentary Basin: The Leading Edge, Vol. 22, No. 7, p. 670–674, 2003.

Nairn AEM and Alsharhan, AS, Sedimentary Basins and Petroleum Geology of the Middle East, Elsevier, Netherlands, 1997.

Neves, F.A., Mustafa, H. M. and Rutty, P.M., Pseudo-gamma Ray Volume from Extended Elastic Impedance Inversion for Gas Exploration: The Leading Edge, Vol. 23, No. 06, p. 536–540, 2004.

Whitcombe, D., Connolly, P., Reagan, R. and Redshaw T., Extended Elastic Impedance for Fluid and Lithology Prediction, Geophysics, Vol. 67, 3999 1, p. 63–67, 2002.